JOURNAL OF ELECTROMAGNETIC ENGINEERING AND SCIENCE, VOL. 22, NO. 5, 599~607, SEP. 2022

https://doi.org/10.26866/jees.2022.5.r.128
ISSN 2671-7263 (Online) · ISSN 2671-7255 (Print)

A Compact Dual-Band MIMO Antenna for Sub-6 GHz 5G Terminals

Guiting Dong · Jianlin Huang · Simin Lin · Zhizhou Chen · Gui Liu*

Abstract

In this paper, a dual-band multiple-input-multiple-output (MIMO) antenna is proposed for fifth-generation (5G) wireless communication terminals. The measured −10 dB impedance bandwidths of 380 MHz (3.34–3.72 GHz) and 560 MHz (4.57–5.13 GHz) can cover the 3.4–3.6 GHz and 4.8–5 GHz 5G bands. The single antenna element of this proposed MIMO is composed of an F-shaped feed strip and an inverted L-shaped radiation strip. A defected ground structure is employed to obtain a good isolation performance, whereby the measured isolation between the antenna elements is observed to be larger than 23 dB. The measured total radiation efficiencies at 3.5 GHz and 4.9 GHz are 76.65% and 71.93%, respectively. Besides, the calculated envelope correlation coefficients (ECC) are less than 0.00125 and 0.01164 at the low-frequency and high-frequency bands, respectively. Furthermore, the specific absorption ratio (SAR) analysis of the antenna verifies that it qualifies for 5G terminals.

Key Words: Dual Band, Fifth-Generation (5G), High-Isolation, MIMO Antenna, Planar Antenna.

I. Introduction

Due to fast-growing wireless communication technologies, fifth-generation (5G) mobile communication systems have been widely rolled out and used in several different applications in recent times. Compared to 4G systems, 5G promises to provide seamless connectivity with higher data rates and lower latency [1]. Two main frequency groups have been adopted in this context—sub-6 GHz and millimeter-wave (mm-wave) bands. Due to their longer wavelength, sub-6 GHz bands have stronger penetration and travel longer distances; as a result, they receive a lot of attention in relation to 5G communication systems.

The ever-increasing data capacity requirements and miniaturization trend of wireless communication devices pose a significant challenge to antenna design in terms of achieving a compact size with high data rate handling capability. An effective way to solve this problem is to adopt multiple-input-multiple-output (MIMO) antenna technology, which improves both spectrum efficiency and data rates [2–4].

For the successful implementation of spatial diversity in a MIMO antenna system, strategies to decrease mutual coupling and improve isolation between the antenna elements are crucial. Many studies have focused on enhancing the isolation of MIMO antennas. Some MIMO antennas achieve good isolation by maintaining an appropriate distance between the antenna elements. In one study [5], mirror-imaged placement of the antenna elements and insertion of a chip inductor between closely spaced antennas were able to improve isolation. Apart from this, grounding branches can generate new coupling and affect isolation [6, 7]. The application of grounded branches can

Manuscript received February 26, 2022 ; Revised May 6, 2022 ; Accepted June 28, 2022. (ID No. 20220226-020J)
College of Electrical and Electronic Engineering, Wenzhou University, Zhejiang, China.
*Corresponding Author: Gui Liu (e-mail: gliu@wzu.edu.cn)

improve isolation in the lower frequency band and provide better impedance matching for the antenna [6]. Furthermore, a neutral line is often employed to weaken mutual coupling [8–10]. Connecting adjacent orthogonal pairs of antennas with a short neutral line leads to high isolation [10].

Additionally, defected ground structures (DGS) can improve isolation by affecting the circuit substrate's effective dielectric constant distribution—this has become a commonly used technology for overcoming undesired coupling in MIMO antenna designs [11–14]. Some MIMO antennas use unique decoupling structures to improve isolation, such as the multi-slot decoupling structure [15], the generic decoupling structure composed of an array of H-shaped parasitic structures [16], and the rectangular microstrip stub [17].

Meanwhile, the antenna proposed in another study [18] used ungrounded full-wavelength strip resonators, which effectively enhanced the isolation between the antenna elements at the cost of reducing the impedance bandwidth. Meta-surface [19, 20] and electromagnetic band gap (EBG) structures [21–23] are also effective methods for improving isolation, although they are too complex to be used in miniaturized antennas. To sum up, the design methodology for achieving good isolation in a small-size MIMO antenna system continues to be a critical issue.

This paper presents a novel decoupling structure that utilizes a DGS to achieve high isolation of more than 23 dB. The DGS includes a rectangular slot with 42 circular slots located on each side. The antenna has a compact size of 28 mm × 28 mm × 0.8 mm, which is suitable for the miniaturization of sub-6 GHz 5G terminals. The proposed MIMO antenna covers both the 3.5 GHz (3.4–3.6 GHz) and 4.9 GHz (4.8–5.0 GHz) frequency bands. Furthermore, the measured total efficiencies at 3.5 GHz and 4.9 GHz are 76.65% and 71.93%, respectively. The calculated envelope correlation coefficients (ECC) is less than 0.00328 in both the desired frequency bands. Moreover, the simulated specific absorption ratio (SAR) values are all observed to be less than 1.4 in the dual bands, thus conforming to the standard for terminal equipment.

II. Antenna Structure

The configuration of the proposed antenna is illustrated in Fig. 1. The antenna elements are etched on an FR4 substrate with $\varepsilon_r = 4.4$ and $\tan\delta = 0.02$, with the size of the substrate being 28 mm × 28 mm × 0.8 mm. The antenna element comprises an inverted L-shaped radiation strip and an F-shaped feeding strip. These two antenna elements are distributed diagonally symmetric to the substrate. Furthermore, each antenna element is fed with a 50-Ω microstrip feedline. The DGS contributes to weakening mutual coupling and enhancing isolation. The detailed dimensions of the antenna element are illustrated in Fig. 1(b).

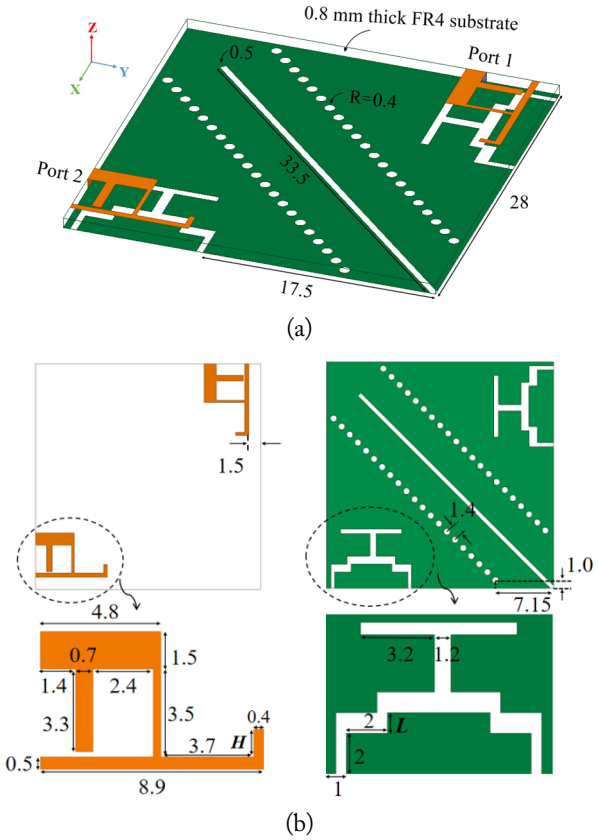

Fig. 1. The geometry of the proposed MIMO: (a) perspective view and (b) detailed dimensions of the antenna element antenna (unit: mm).

III. Antenna Analysis

1. Design Evolution

Fig. 2 depicts the methodology for the design evolution of a

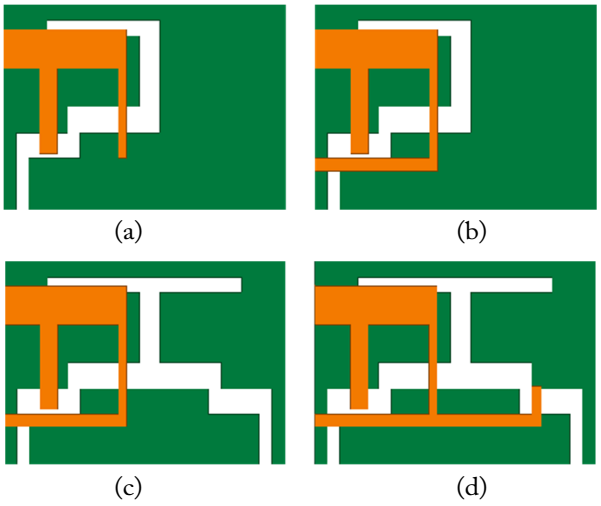

Fig. 2. The design evolution of a single MIMO antenna element: (a) Ant-1, (b) Ant-2, (c) Ant-3, and (d) Ant-4 (proposed antenna).

single MIMO antenna element. As shown in Fig. 3, the F-shaped structure of Ant-1 generates resonance in the lower frequency band. Ant-2, which is obtained by adding a rectangular patch to Ant-1, can excite two modified resonate modes. Meanwhile, Ant-3 modifies the etched slots of the ground plane and generates a symmetrical ground slot structure, which can change the antenna element's distribution parameters—reducing its distributed capacitance and resistance. Therefore, although Ant-3 enhances the resonance of the two bands, it has a negative effect on impedance matching. In Ant-4, however, the addition of the inverted L-shaped radiation strip improves the performance, enabling it to achieve qualified performance in both the desired frequency bands, which are 3.4–3.6 GHz and 4.8–5 GHz. The impedance of the different antenna structures, as shown in Fig. 4, shows the L-shaped radiation strip of Ant-4 increases resistance and achieves better impedance matching within the desired frequency bands.

2. Dimension Optimization

The surface current distributions of a single antenna element are depicted in Fig. 5. The surface current of 3.5 GHz is concentrated on the L-shaped radiation strip; hence, the resonance

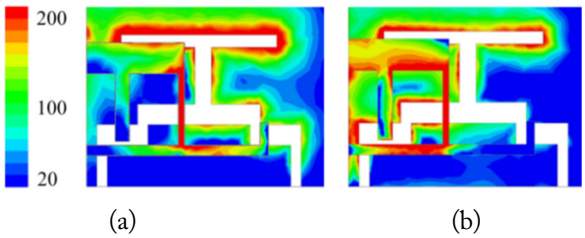

Fig. 5. The surface current distributions of the proposed antenna at (a) 3.5 GHz and (b) 4.9 GHz (unit: A/m).

of the 3.5 GHz band can be effectively adjusted by changing the length of the L-shaped radiation strip. Meanwhile, Fig. 5(b) depicts that the current at 4.9 GHz is concentrated on the F-shaped feed strip and its corresponding ground slot structure. Therefore, modifying the structure of the slot at the corresponding position can significantly affect the performance of the antenna in the higher frequency band.

The simulated S_{11} parameters of different values of H and L (as shown in Fig. 1) are depicted in Figs. 6 and 7—verifying the above analysis derived from the surface current distributions. By increasing the length H of the L-shaped radiation strip, the lower resonant frequency of the antenna can be moved to higher

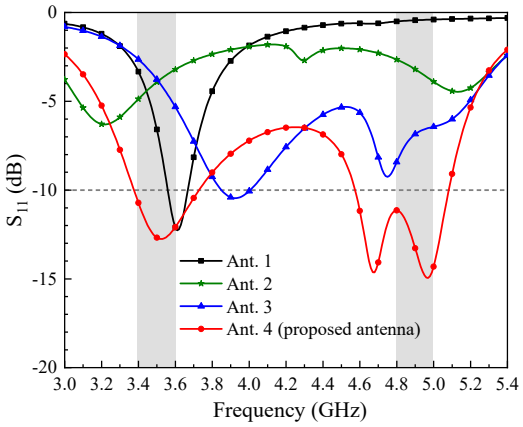

Fig. 3. S_{11} of the various antennas.

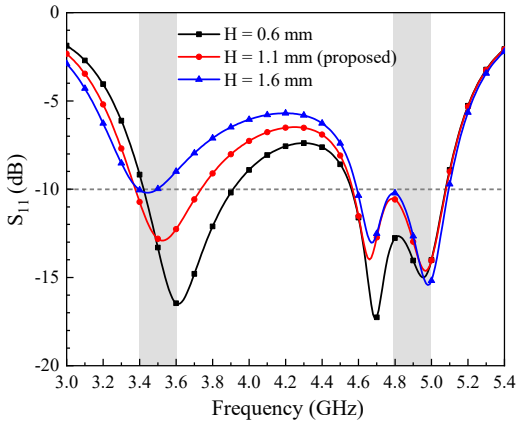

Fig. 6. Simulated S_{11} with different values of H.

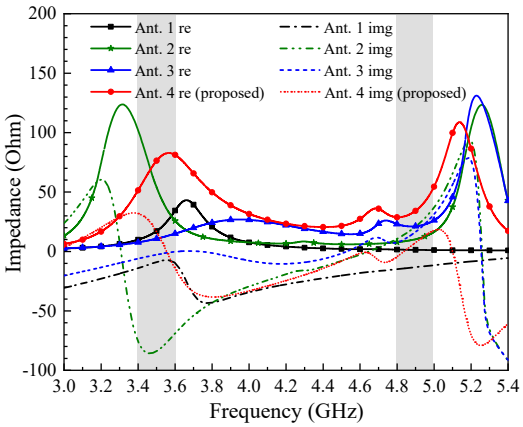

Fig. 4. Comparison of the impedance of the various antennas.

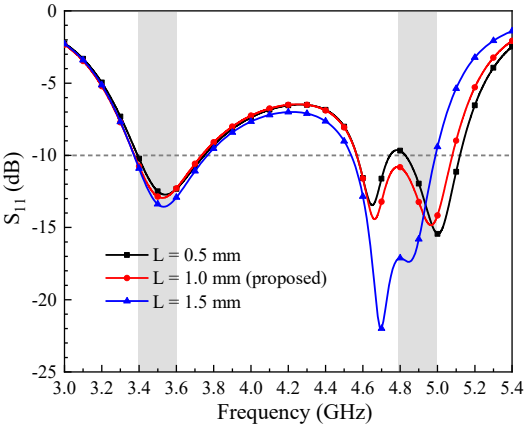

Fig. 7. Simulated S_{11} with different values of L.

frequencies. Meanwhile, when adjusting the value of L, the distribution parameters of the antenna elements will also change accordingly, effectively widening the operating band in the 4.9 GHz band. It is evident that when L = 1.0 mm and H = 1.1 mm, the desired frequency bands will be sufficiently covered.

3. Isolation Optimization

As depicted in Fig. 8, this study proposes different isolation structures—Structure 1, Structure 2, and Structure 3—to achieve better isolation performance. Compared to Structure 1, Structure 2 adds a diagonal rectangular slot, which improves antenna isolation to be more than −20 at the higher frequency band. Twenty-one circular slots are evenly distributed on both sides of the diagonal rectangular slot in Structure 3. The circular slots in the ground can improve high-frequency isolation while also broadening the bandwidth of the antenna in the higher frequency band. The slotted-dot lines broaden the −10 dB bandwidth from 4.8–5.07 GHz to 4.57–5.07 GHz, enabling the antenna to exhibit a more stable performance in the required 4.8–5.0 GHz band. The simulated *S*-parameters of the three isolation structures are shown in Fig. 9. Notably, the isolation of the proposed antenna is more than 22 dB in both the desired frequency bands.

4. 3D Radiation Pattern

Fig. 10 presents the 3D radiation pattern of a single antenna element by inducing excitation at one port while keeping the other port terminated using a matching load. The simulated 3D radiation patterns show that the proposed antenna achieves a maximum gain of 1.99 dB at 3.5 GHz and 2.12 dB at 4.9 GHz.

Fig. 8. Different isolation structures: (a) Structure 1, (b) Structure 2, and (c) Structure 3.

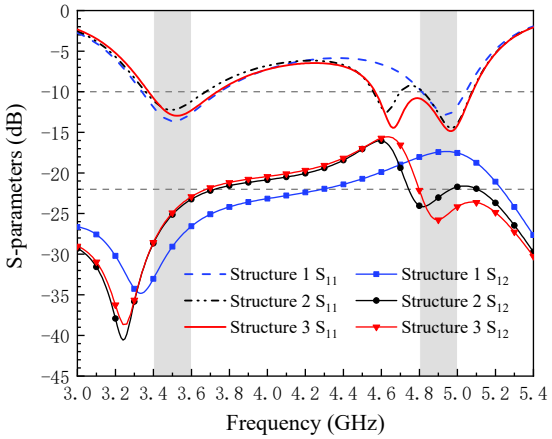

Fig. 9. Simulated *S*-parameters of the different isolation structures.

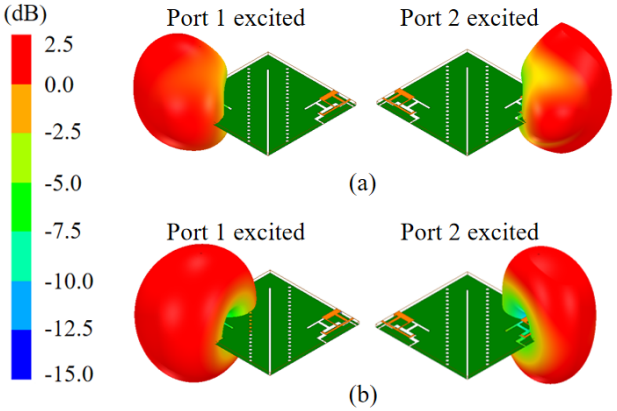

Fig. 10. The 3D radiation patterns of the single element at (a) 3.5 GHz and (b) 4.9 GHz.

IV. Experimental Analysis

Following the design process, the antenna prototype was manufactured, the photograph of which is illustrated in Fig. 11. Fig. 12 shows the specific circumstances of the measured and

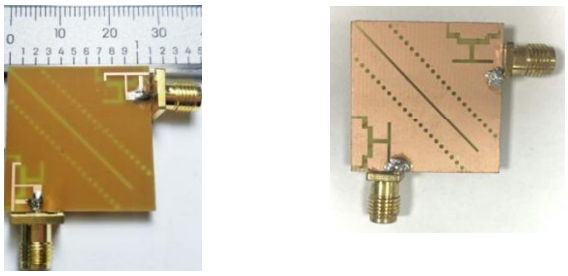

Fig. 11. Photograph of the antenna prototype: (a) top view and (b) bottom view.

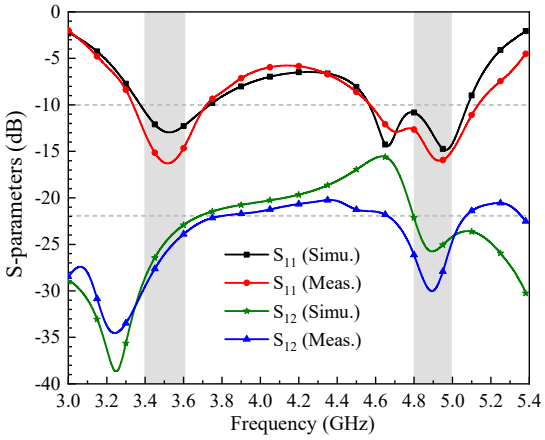

Fig. 12. Simulated and measured *S*-parameters of the MIMO system.

simulated *S*-parameters of the proposed antenna. The measured −10 dB impedance bandwidths are 380 MHz (3.34–3.72 GHz) and 560 MHz (4.57–5.13 GHz), which can sufficiently cover the 3.5 GHz (3.4–3.6 GHz) and 4.9 GHz (4.8–5 GHz) frequency bands. Furthermore, the measured and simulated isolation is also more than 23 dB and 22 dB, respectively.

The measured and simulated radiation patterns at both 3.5 GHz and 4.9 GHz are demonstrated in Fig. 13, where Port 1 is excited while Port 2 is terminated by a 50-Ω matching load. The overall trend of the measured and simulated results is similar, while reasonable discrepancy is observed to be caused by the manufacturing process and proximity effect of the test setup (e.g., connectors, cables, and positioners).

Fig. 14 illustrates the simulated and measured peak gains and total radiation efficiencies. The measured peak gains at 3.5 GHz and 4.9 GHz are 2 dBi and 2.46 dBi, respectively. Meanwhile, the total efficiencies at 3.5 GHz and 4.9 GHz are 76.65% and 71.93%, respectively. The results, therefore, exhibit good consistency between the simulated and measured peak gains and total efficiencies.

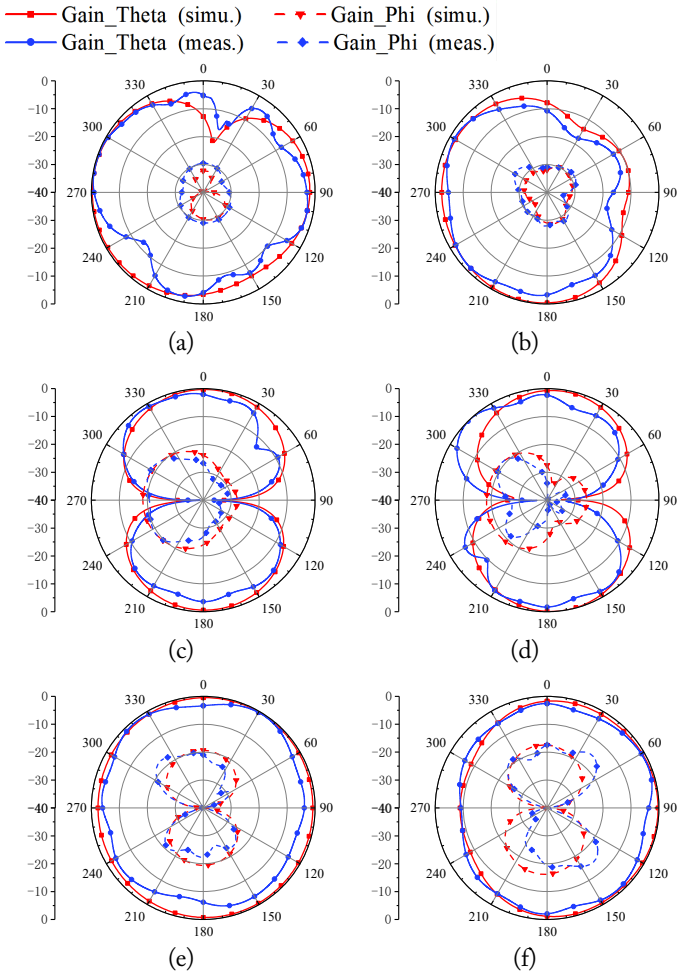

Fig. 13. Simulated and measured radiation patterns of the proposed antenna: (a) xoy plane, (c) yoz plane, (e) xoz plane at 3.5 GHz and (b) xoy plane, (d) yoz plane, (f) xoz plane at 4.9 GHz.

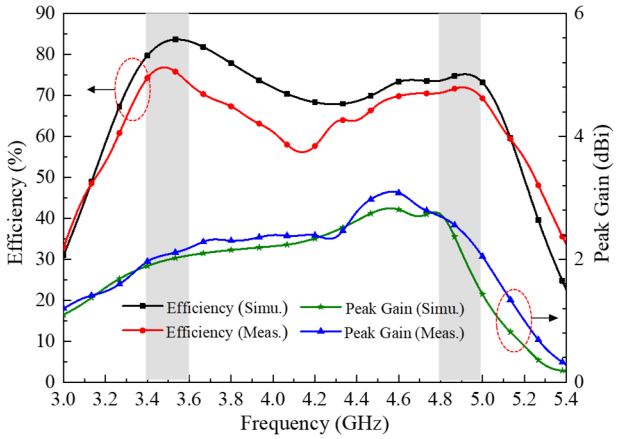

Fig. 14. Simulated and measured peak gain and total efficiencies of the proposed MIMO antenna.

To further investigate the antenna performance, the ECC is calculated according to the far-field radiation patterns—expressed by Eq. (1).

$$\rho_e = \frac{\left|\iint_{4\pi}[F_1(\theta,\varphi)\cdot F_2(\theta,\varphi)]d\Omega\right|^2}{\iint_{4\pi}|F_1(\theta,\varphi)|^2\,d\Omega\iint_{4\pi}|F_2(\theta,\varphi)|^2 d\Omega} \tag{1}$$

where $F_i(\theta,\varphi)$ represents the radiation pattern when port i is excited, and Ω represents the solid angle.

The ECC calculation method using the *S*-parameters—a widely used process—is obtained from Eq. (2):

$$\rho_e = \frac{|S_{11}^* S'_{12} + S_{21}^* S'_{22}\ |^2}{(1-|S_{11}|^2-|S_{21}|^2)(1-|S_{22}|^2-|S_{12}|^2)} \tag{2}$$

where S^* represents the imaginary part of the *S*-parameters, while S' represents their real part.

The calculated ECC is presented in Fig. 15. Since Eq. (2) considers only the isolation between the antenna input ports and does not take the coupling between the radiation fields into account, the obtained result is not as accurate as Eq. (1). The

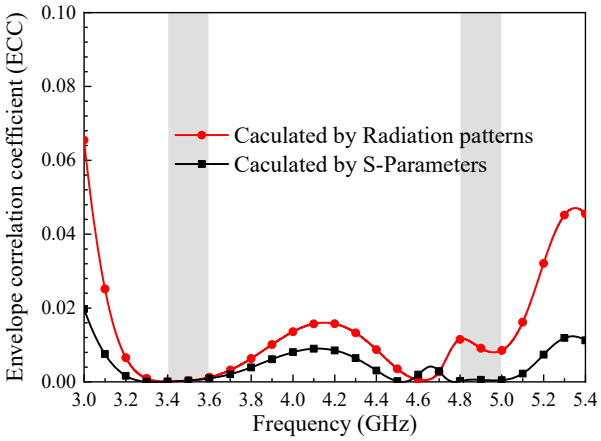

Fig. 15. Calculated ECC of the MIMO antenna system.

ECC calculated by the radiation patterns turns out to be less than 0.00125 and 0.01164 at the 3.5 GHz and 4.9 GHz bands, respectively. The calculated ECC is far smaller than the acceptable threshold of 0.3, meaning that the antenna system exhibits good diversity performance.

V. Effect on Users and SAR Investigation

In the case of a 5G terminal antenna, it is necessary to consider the effects of the human body on the antenna. Hence, this section simulates the working conditions of the antenna on the human wrist, as shown in Fig. 16.

The simulated S_{11} values of the proposed antenna on the wrist are illustrated in Fig. 17. Although there are a few changes in the reflectance coefficients in the 3.5 GHz and 4.9 GHz bands, they still meet the requirements of the two bands. The overall trend in free space and the wrists is consistent due to the ground at the bottom. Fig. 18 shows the 3D radiation patterns of the proposed MIMO system on the wrist. The proposed MIMO antenna retains an adequate gain and a good radiation pattern.

The SAR indicates the impact of device radiation on the human body, with a low SAR value demonstrating weak absorption of radiation by the human body. Fig. 19 shows a SAR simulation of the antenna on the wrist at 3.5 GHz and 4.9 GHz. The distance between the antenna and the wrist in this simulation is less than 4 mm. The results show that the 1 g average SAR values are less than 1.34 W/kg and 1.4 W/kg at 3.5 GHz and 4.9 GHz, respectively. Thus, the SAR level of the proposed antenna meets the standards of 1.6 W/kg per 1 g tissue in the United States.

Table 1 depicts a performance comparison of the proposed MIMO antenna and other reported antennas, highlighting the good isolation and compact structure of the former.

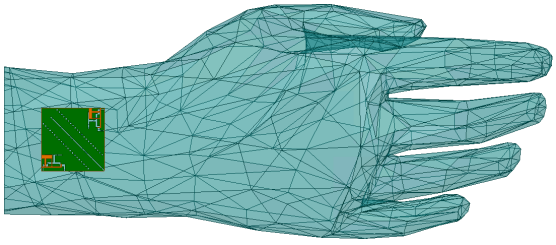

Fig. 16. The model of the proposed antenna working on the wrist.

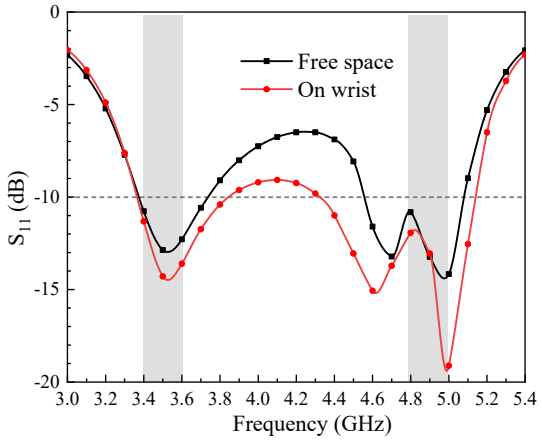

Fig. 17. Simulated S_{11} of the proposed antenna on the wrist.

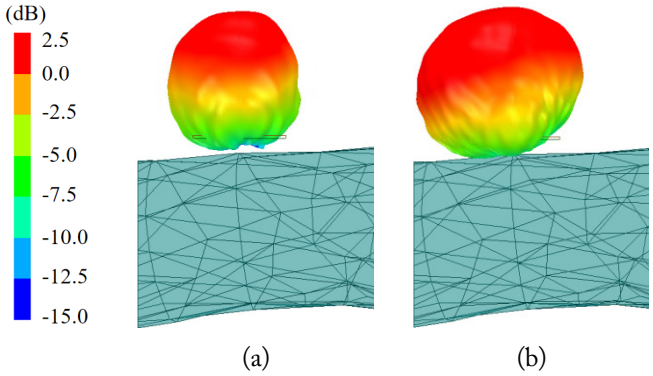

Fig. 18. The 3D radiation patterns of the proposed antenna on the wrist at (a) 3.5 GHz and (b) 4.9 GHz.

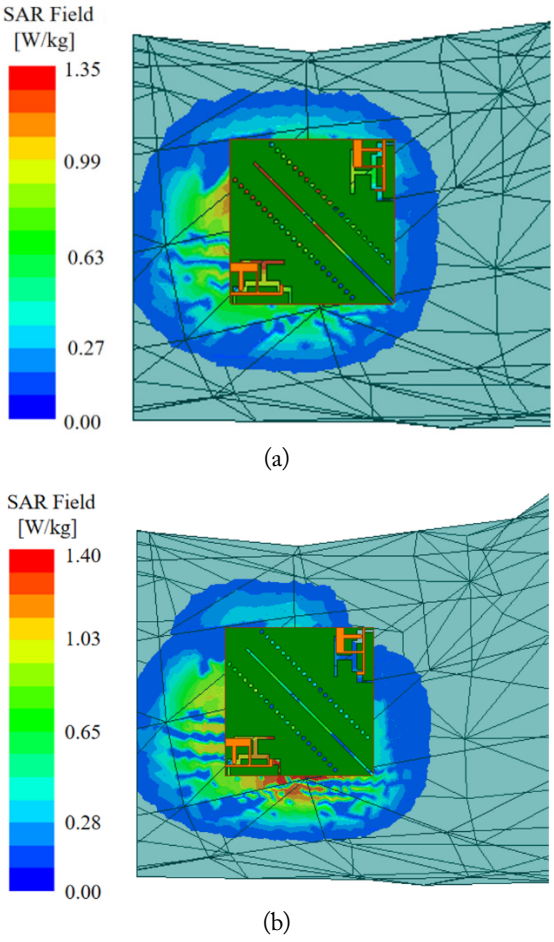

Fig. 19. Simulated SAR at (a) 3.5 GHz and (b) 4.9 GHz.

Table 1. Comparison of the proposed MIMO antenna and other reported antennas

Study	Operating bands (GHz)	Isolation (dB)	Peak gain (dBi)	ECC	Size
Ameen et al. [3]	3.4–3.6	−11	3.25	0.003	$0.24\lambda_0 \times 0.54\lambda_0 \times 0.019\lambda_0$ @ 3.54 GHz
	4.0–8.0	−15	3.4		
Boukarkar et al. [4]	3.471–3.529	−18.4	2.7	0.08	$0.41\lambda_0 \times 0.41\lambda_0 \times 0.04\lambda_0$ @ 3.5 GHz
	5.678–5.721	−22.7	2.85		
Wang et al. [6]	3.409–3.601	−22.3	2.45	0.005	$0.45\lambda_0 \times 0.66\lambda_0 \times 0.017\lambda_0$ @ 3.5 GHz
	4.76–5.04	−30.8	4.56		
Ren and Zhao [7]	3.4–3.6	−17.5	6.03	0.14	$1.75\lambda_0 \times 0.88\lambda_0 \times 0.009\lambda_0$ @ 3.5 GHz
	4.8–5.0	−20	8.17	0.12	
Proposed	3.34–3.72	−22	2.0	0.00125	$0.33\lambda_0 \times 0.33\lambda_0 \times 0.009\lambda_0$ @ 3.5 GHz
	4.57–5.13	−21	2.46	0.01164	

VI. Conclusion

A dual-band MIMO antenna operating in the 3.5 GHz band (3.4–3.6 GHz) and 4.9 GHz band (4.8–5 GHz) is presented in this study. The design evolution and dimension optimization of the single antenna element are analyzed to optimize antenna performance. The measured isolation of the antenna is observed to be more than 23 dB. The total efficiencies at 3.5 GHz and 4.9 GHz are about 76.65% and 71.93%, respectively. The results of the SAR analysis, simulated for the proposed terminal antenna, also meet the standard for terminal devices. Moreover, the measurement results are consistent with the simulation. Therefore, it can be concluded that the proposed MIMO antenna is a good candidate for use in 5G wireless communication systems.

This study was funded in part by the National Natural Science Foundation of China (No. 61671330), the Science and Technology Department of Zhejiang Province (No. LGG19F010009), and the Wenzhou Municipal Science and Technology Program (No. C20170005 and 2018Z G019).

References

[1] M. R. Palattella, M. Dohler, A. Grieco, G. Rizzo, J. Torsner, T. Engel, and L. Ladid, "Internet of Things in the 5G era: enablers, architecture, and business models," *IEEE Journal on Selected Areas in Communications*, vol. 34, no. 3, pp. 510-527, 2016.

[2] M. I. Khan, M. I. Khattak, and M. M. Al-Hasan, "Miniaturized MIMO antenna with low inter-radiator transmittance and band rejection features," *Journal of Electromagnetic Engineering and Science*, vol. 21, no. 4, pp. 307-315, 2021.

[3] M. Ameen, O. Ahmad, and R. K. Chaudhary, "Single split-ring resonator loaded self-decoupled dual-polarized MIMO antenna for mid-band 5G and C-band applications," *AEU-International Journal of Electronics and Communications*, vol. 124, article no. 153336, 2020. https://doi.org/10.1016/j.aeue.2020.153336

[4] A. Boukarkar, X. Q. Lin, Y. Jiang, L. Y. Nie, P. Mei, and Y. Q. Yu, "A miniaturized extremely close-spaced four-element dual-band MIMO antenna system with polarization and pattern diversity," *IEEE Antennas and Wireless Propagation Letters*, vol. 17, no. 1, pp. 134-137, 2018.

[5] S. C. Chen, C. W. Chiang, and C. I. G. Hsu, "Compact four-element MIMO antenna system for 5G laptops," *IEEE Access*, vol. 7, pp. 186056-186064, 2019.

[6] W. Wang, Y. Wu, W. Wang, and Y. Yang, "Isolation enhancement in dual-band monopole antenna for 5G applications," *IEEE Transactions on Circuits and Systems II: Express Briefs*, vol. 68, no. 6, pp. 1867-1871, 2021.

[7] Z. Ren and A. Zhao, "Dual-band MIMO antenna with compact self-decoupled antenna pairs for 5G mobile applications," *IEEE Access*, vol. 7, pp. 82288-82296, 2019.

[8] M. Li, L. Jiang, and K. L. Yeung, "A general and systematic method to design neutralization lines for isolation enhancement in MIMO antenna arrays," *IEEE Transactions on Vehicular Technology*, vol. 69, no. 6, pp. 6242-6253, 2020.

[9] S. Wang and Z. Du, "Decoupled dual-antenna system using crossed neutralization lines for LTE/WWAN smartphone applications," *IEEE Antennas and Wireless Propagation Letters*, vol. 14, pp. 523-526, 2014.

[10] D. Serghiou, M. Khalily, V. Singh, A. Araghi, and R. Tafazolli, "Sub-6 GHz dual-band 8 × 8 MIMO antenna for 5G smartphones," *IEEE Antennas and Wireless Propa-*

gation Letters, vol. 19, no. 9, pp. 1546-1550, 2020.

[11] P. Ramanujam, P. R. Venkatesan, C. Arumugam, and M. Ponnusamy, "Design of miniaturized super wideband printed monopole antenna operating from 0.7 to 18.5 GHz," *AEU-International Journal of Electronics and Communications*, vol. 123, article no. 153273, 2020. https://doi.org/10.1016/j.aeue.2020.153273

[12] C. Y. Chiu, F. Xu, S. Shen, and R. D. Murch, "Mutual coupling reduction of rotationally symmetric multiport antennas," *IEEE Transactions on Antennas and Propagation*, vol. 66, no. 10, pp. 5013-5021, 2018.

[13] R. Yang, S. Xi, Q. Cai, Z. Chen, X. Wang, and G. Liu, "A compact planar dual-band multiple-input and multiple-output antenna with high isolation for 5G and 4G applications," *Micromachines*, vol. 12, no. 5, article no. 544, 2021. https://doi.org/10.3390/mi12050544

[14] H. Peng, R. Zhi, Q. Yang, J. Cai, Y. Wan, and G. Liu, "Design of a MIMO antenna with high gain and enhanced isolation for WLAN applications," *Electronics*, vol. 10, no. 14, article no. 1659, 2021. https://doi.org/10.3390/electronics10141659

[15] W. Hu, L. Qian, S. Gao, L. H. Wen, Q. Luo, H. Xu, X. Liu, Y. Liu, and W. Wang, "Dual-band eight-element MIMO array using multi-slot decoupling technique for 5G terminals," *IEEE Access*, vol. 7, pp. 153910-153920, 2019.

[16] M. Abdullah and S. Koziel, "A novel versatile decoupling structure and expedited inverse-model-based re-design procedure for compact single-and dual-band MIMO antennas," *IEEE Access*, vol. 9, pp. 37656-37667, 2021.

[17] Y. Dou, Z. Chen, J. Bai, Q. Cai, and G. Liu, "Two-port CPW-fed dual-band MIMO antenna for IEEE 802.11 a/b/g applications," *International Journal of Antennas and Propagation*, vol. 2021, article no. 5575887, 2021. https://doi.org/10.1155/2021/5572887

[18] S. C. Chen, L. C. Chou, C. I. Hsu, and S. M. Li, "Compact sub-6-GHz four-element MIMO slot antenna system for 5G tablet devices," *IEEE Access*, vol. 8, pp. 154652-154662, 2020.

[19] R. Mark, N. Rajak, K. Mandal, and S. Das, "Metamaterial based superstrate towards the isolation and gain enhancement of MIMO antenna for WLAN application," *AEU-International Journal of Electronics and Communications*, vol. 100, pp. 144-152, 2019.

[20] F. Liu, J. Guo, L. Zhao, G. L. Huang, Y. Li, and Y. Yin, "Dual-band metasurface-based decoupling method for two closely packed dual-band antennas," *IEEE Transactions on Antennas and Propagation*, vol. 68, no. 1, pp. 552-557, 2020.

[21] K. S. Parvathi and S. R. Gupta, "Novel dual-band EBG structure to reduce mutual coupling of air gap based MIMO antenna for 5G application," *AEU-International Journal of Electronics and Communications*, vol. 138, article no. 153902, 2021. https://doi.org/10.1016/j.aeue.2021.153902

[22] J. P. Shinde and P. N. Shinde, "M-shape electromagnetic-bandgap structures for enhancement in antenna performance," *AEU-International Journal of Electronics and Communications*, vol. 70, no. 6, pp. 842-849, 2016.

[23] P. P. Bhavarthe, S. S. Rathod, and K. T. V. Reddy, "A compact dual band gap electromagnetic band gap structure," *IEEE Transactions on Antennas and Propagation*, vol. 67, no. 1, pp. 596-600, 2019.

Guiting Dong

was born in Sichuan, China, in 1997. She received her B.S. degree in Electrical Engineering from Shanghai University of Electric Power in 2019. She is currently pursuing her M.S. degree at Wenzhou University. Her research interests include multiband antennas, MIMO technologies, and RFIC design.

Zhi-Zhou Chen

received his B.S. degree in Integrated Circuit Design and Integration System from Hangzhou Dianzi University, Hangzhou, China, in 2010, and his M.S. and Ph.D. degrees in Circuits and Systems from Shanghai Institute of Technical Physics, Chinese Academy of Sciences, in 2015 and 2017, respectively. Since 2017, he has been a lecturer at the College of Electrical and Electronic Engineering at Wenzhou University. His research interests include antenna design and photoelectric sensing methods and systems.

Jianlin Huang

was born in Zhejiang, China, in 1995. He received his B.S. degree in Electrical Engineering from Wenzhou University in 2018. He is currently pursuing his M.S. degree at Wenzhou University. His research interests include antenna and RFIC design.

Gui Liu

was born in Wenzhou, Zhejiang, China, in 1975. He received his B.S. degree in Communication Engineering from South China University of Technology, Guangdong, China, in 1997, and his M.S. degree in Electrical Engineering from Sun Yat-Sen University, Guangdong, China, in 2003. In 2011, he received his Ph.D. degree in Electrical Engineering from the Illinois Institute of Technology, Chicago, IL, USA. Since September 2011, he has been a professor at Wenzhou University in China. He is currently a full professor and Oujiang Distinguished Professor at the College of Electrical and Electronic Engineering at Wenzhou University. His research interests include antennas, millimeter-wave on-chip passive components, and RFIC design. He serves as an active reviewer for numerous IEEE, Elsevier, IOP Science, and other international journals.

Simin Lin

was born in Fujian, China, in 2001. She is currently pursuing her B.S. degree at Wenzhou University. Her research interests include multiband antenna and MIMO antenna design.